

Effect of BMIM-BF4 Concentration in Water on the Lift Force Coefficient of Rising Single Bubbles

Djamel Eddine Aissaoui[1], Nicolò Varallo[1], Lantian Wang[2], Hendrik Hessenkemper[2], Giorgio Besagni[1,2]

[1] Politecnico di Milano, Department of Energy, Milan, Italy [2] Helmholtz-Zentrum Dresden-Rossendorf, Institute of Fluid Dynamics, Dresden, Germany

22nd Multiphase Flow Workshop (MPF 2026), HZDR, Dresden, 2–6 November 2026

Outline

1. **Motivation**
   - AURIGA, ionic liquids and the lift closure gap
   - Lift force mechanisms in clean and contaminated liquids
2. **Methodology**
   - Experiment and fluids
   - Force balance, processing and validation
3. **Results**
   - Lift coefficient versus size; concentration effect
   - Shape and the reversal criterion
4. **Discussion**
   - The limit of the interface analysis and the second liquid, EMIM-Ac
   - Other candidate mechanisms
5. **Conclusions and Outlook**

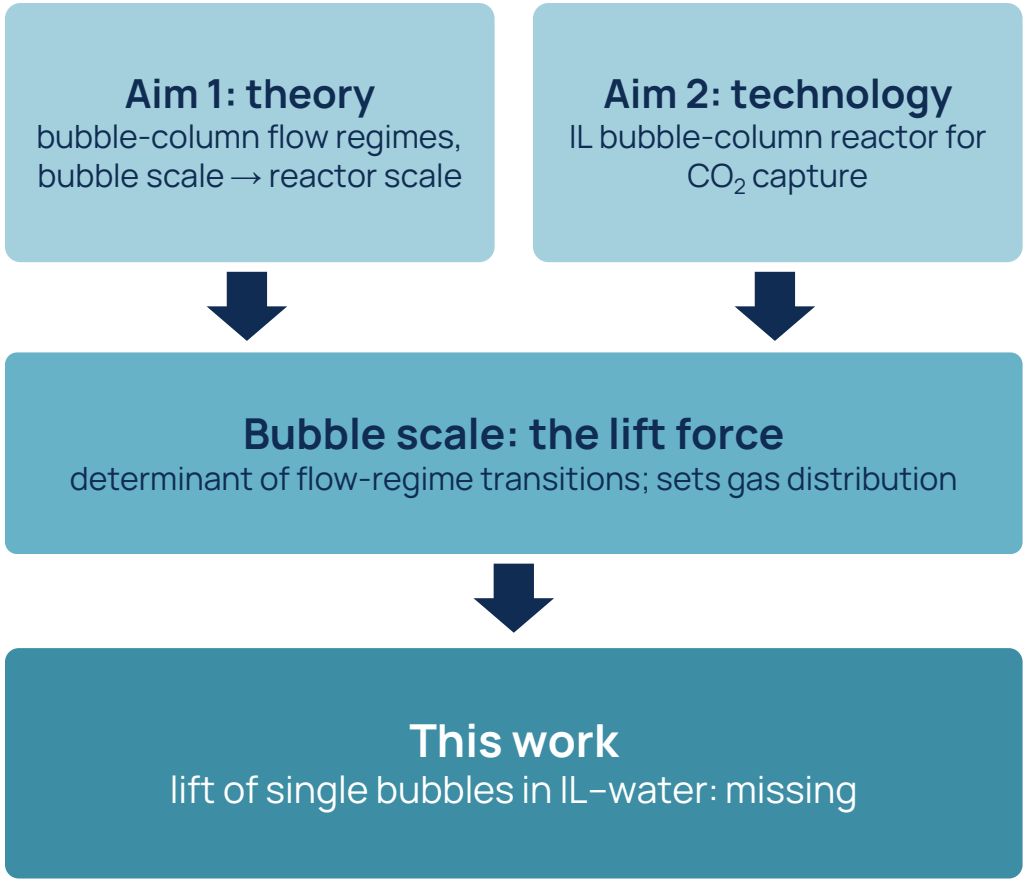
Motivation: AURIGA and Ionic-Liquid CO_2 Capture

[1] Shah et al. 1982
[2] Lucas et al. 2005; Lucas & Ziegenhein 2019

AURIGA has two long-term aims:

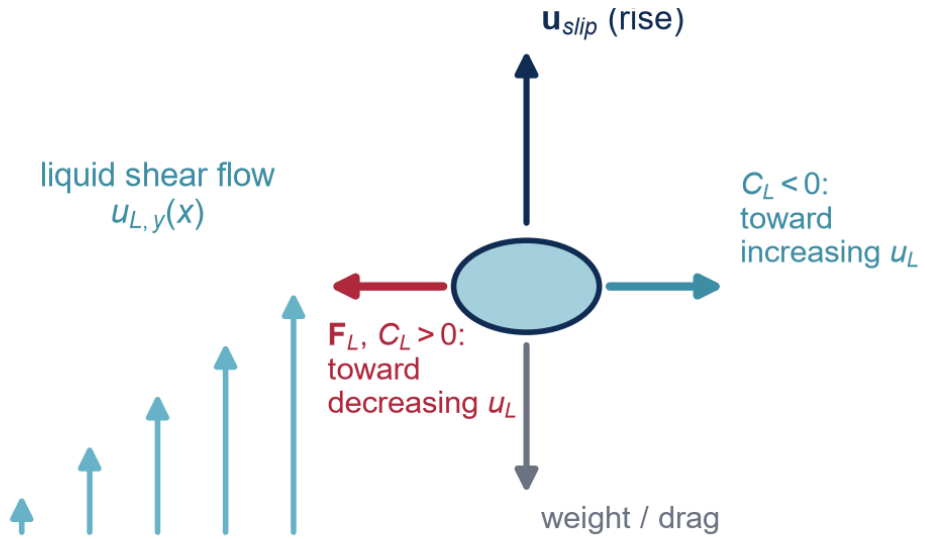
- Aim 1, theory: flow regimes of bubble columns
- Aim 2, technology: ionic-liquid bubble column for CO2 capture

- Ionic liquids: non-volatile, tunable, potentially lower energy use
- Why regimes matter: they set gas holdup, interfacial area and mixing, hence CO2 transfer and scale-up [1]; the lift force governs the transitions [2]
- **Gap: no lift closure for IL–water mixtures**



Motivation: Lift Force and the Closure Gap

- In AURIGA's theory the bubble-scale lift force is a determinant of flow-regime transitions [1]
- Lift on a bubble: $F_L = -C_L \rho_L V (u_{slip} \times \omega_L)$
- The sign of C_L sets lateral migration: $C_L > 0$ toward decreasing liquid velocity, $C_L < 0$ toward increasing liquid velocity [2]
- Standard lift correlations [3] were derived for water and viscous liquids; the liquid viscosity also affects bubble-column fluid dynamics [4]
- Contaminants change C_L in a complex way that depends on surfactant concentration and type [5]



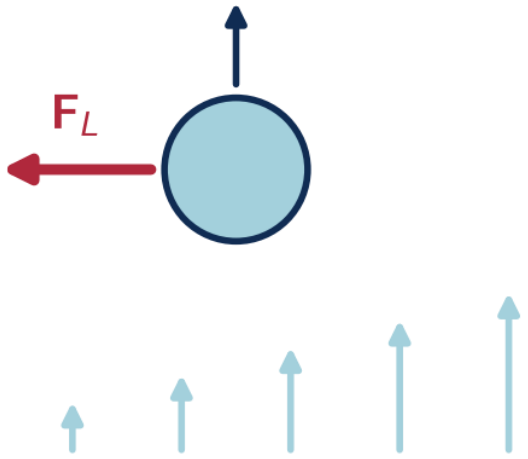
[1] Lucas et al. 2005; Lucas & Ziegenhein 2019
[2] Tomiyama et al. 2002
[3] Tomiyama et al. 2002; Hessenkemper et al. 2021a
[4] Besagni et al. 2017
[5] Hessenkemper et al. 2021b; Takagi & Matsumoto 2011

Research question: how does BMIM-BF_4 concentration change C_L of single bubbles, and why?

Lift Force Mechanisms: Three Regimes

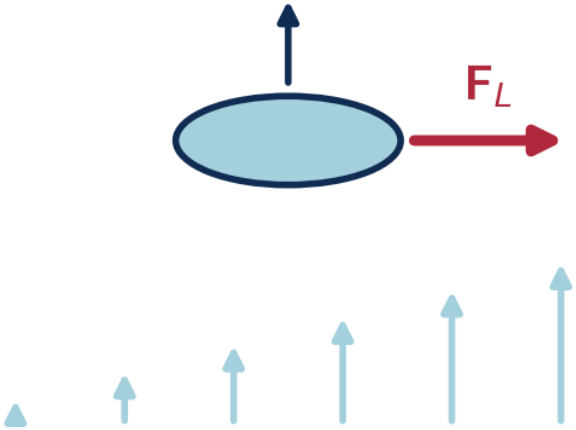
[1] Auton 1987; Legendre & Magnaudet 1998
[2] Adoua et al. 2009; Magnaudet & Eames 2000; Hidman et al. 2022
[3] Cuenot et al. 1997; Takagi & Matsumoto 2011; Hayashi et al. 2020

clean, near-spherical:
tilting + stretching of ambient vorticity
$C_L \to 1/2$



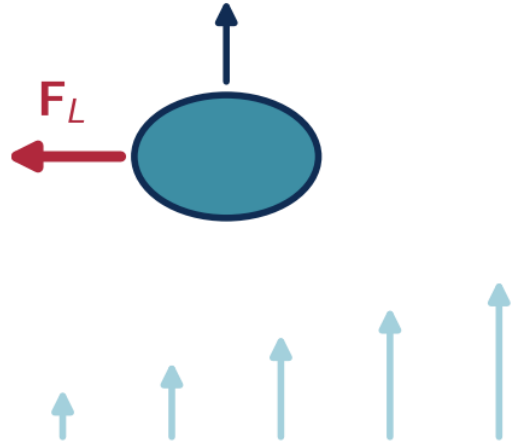
Tilting and stretching of the ambient vorticity: $C_L \to ½$ at high Re [1]

clean, oblate ($\chi \gtrsim 2.2$):
surface vorticity reverses the sign
$C_L < 0$



Vorticity from the free surface forms counter-rotating wake vortices and reverses C_L for $\chi \gtrsim 2.2$ [2]

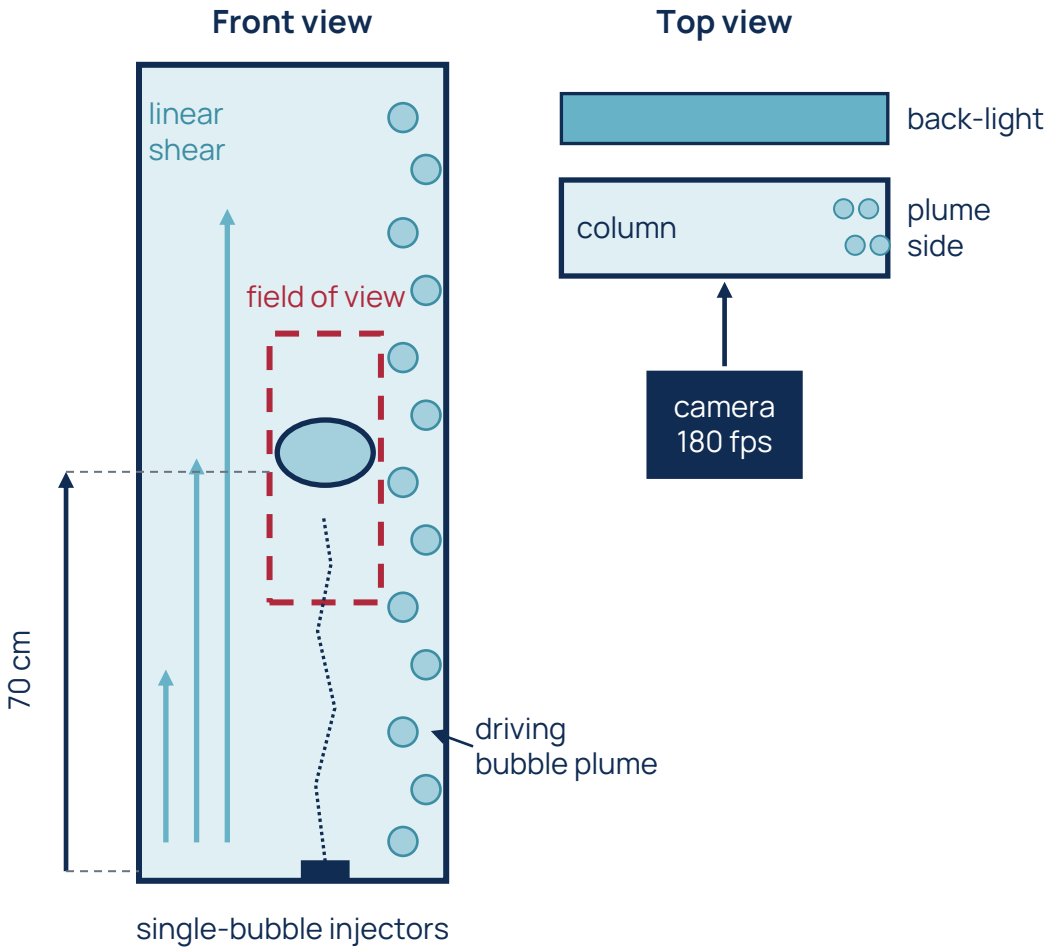
immobilised (contaminated) interface:
rigid-sphere-like, no free-slip
$C_L \approx$ rigid sphere



Adsorbed species cause Marangoni stresses that immobilise the surface [3]

Methodology: Experimental Setup

[1] Ziegenhein et al. 2018

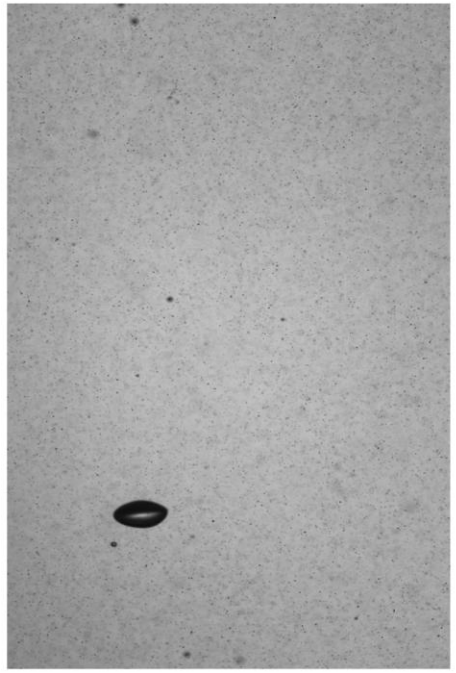


- Single air bubbles rise through a linear shear flow ($\approx 2.1\ s^{-1}$) generated by a driving bubble plume at the column side [1]
- Measurement window 70 cm above the injection: same rise distance for all bubbles
- Five injectors with inner diameters of 0.5 / 1.3 / 2.8 / 5 / 5.8 mm generate bubbles of d_B = 2–6.5 mm
- Particle Shadow Velocimetry (PSV): back-lit images, 180 fps, 1280 × 1920 px, image pairs 5.6 ms apart
- Liquid velocity from tracer particles; bubbles from the same images
- Three repetitions per condition; 15 000–20 000 image pairs per case

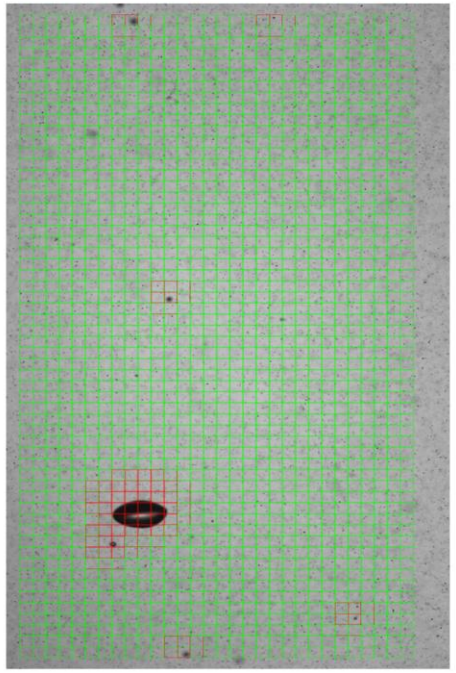
Methodology: Liquid- and Gas-Phase Image Processing

PSV: liquid velocity (one image pair)

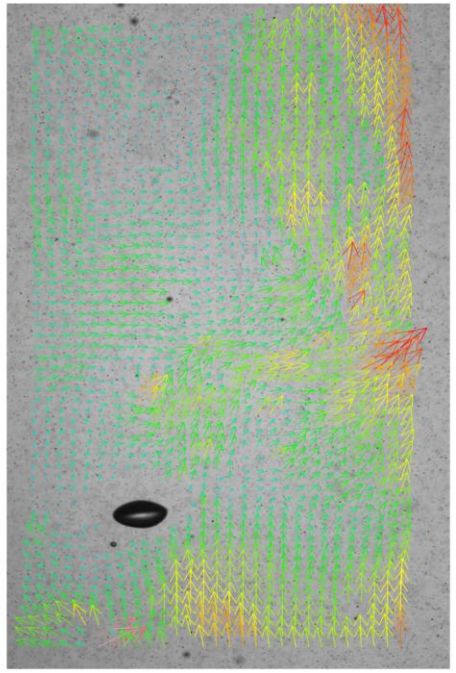
1 Shadow image



2 PSV windows (red: masked)

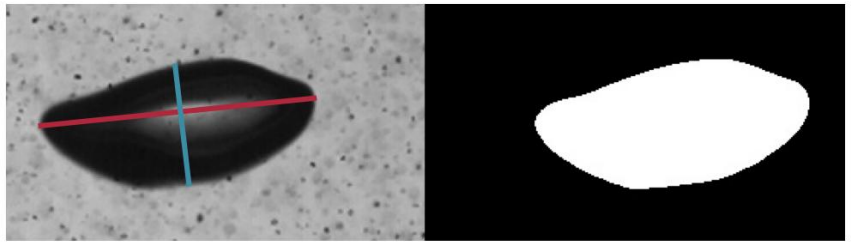


3 Liquid velocity vectors

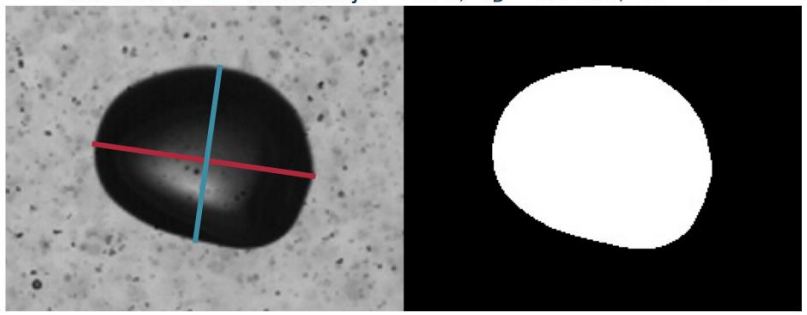


Detection: bubble axes and mask

frame 459: E = minor/major = 0.43, d_B = 6.0 mm, tilt = 7°



frame 294: E = minor/major = 0.79, d_B = 5.9 mm, tilt = -15°



Methodology: Fluids and Interface Properties

Liquid	ρ [kg/m³]	μ [mPa·s]	σ [mN/m]	$\log_{10}$ Mo
BMIM-BF_4 0.1 wt %	997.0	0.890	72.0	−10.78
BMIM-BF_4 1 wt %	998.4	0.952	69.8	−10.63
BMIM-BF_4 5 wt %	1005.0	0.934	59.1	−10.44
BMIM-BF_4 10 wt %	1013.4	1.158	51.3	−9.89
EMIM-Ac 0.1 wt %	997.0	0.890	72.0	−10.78
EMIM-Ac 1 wt %	998.0	0.984	75.9	−10.68
EMIM-Ac 5 wt %	1003.0	1.015	72.7	−10.57
EMIM-Ac 10 wt %	1009.5	1.416	69.5	−9.93

Properties measured in-house at 25 °C; the 0.1 wt % cases use water values (approximation). Mo = $g\,\mu^4\,\Delta\rho\,/\,(\rho^2\,\sigma^3)$.

Methodology: Force Balance

[1] Auton 1987
[2] Ziegenhein et al. 2018; Hessenkemper et al. 2020

$$\mathbf{F}_L = -C_L \rho_L V \left(\mathbf{u}_{slip} \times \boldsymbol{\omega}_L\right), \qquad \boldsymbol{\omega}_L = \nabla \times \mathbf{u}_L$$

$$\textit{vertical:} \qquad (\rho_L - \rho_G) V g = \frac{1}{2} \rho_L C_D A \left|\mathbf{u}_{slip}\right|^2 \qquad \Rightarrow \qquad C_D = \frac{4}{3} \frac{\Delta\rho}{\rho_L} \frac{g d_B}{\left|\mathbf{u}_{slip}\right|^2}$$

$$\textit{horizontal:} \qquad C_L = \frac{\frac{1}{2}\left(\partial_y v_y + \partial_x v_x\right) v_x + \frac{3}{4} \frac{C_D}{d_B} \left|\mathbf{u}_{slip}\right| u_{slip,x}}{u_{slip,y} \omega_z}$$

- $u_{slip} = u_G - u_L$; ω_z from the PSV liquid field including the weak sideways flow $\partial u_x/\partial y \approx -0.24\ s^{-1}$
- d_B and C_D cancel in C_L: only slip velocities, bubble velocity gradients and ω_z enter
- Added-mass coefficient $C_{AM} = 0.5$ (sphere [1]). The added-mass term, the first in the numerator, changes C_L by less than 0.005 in every case (median 0.2 % of the drag): quasi-steady lift–drag balance [2]

Methodology: Processing Chain

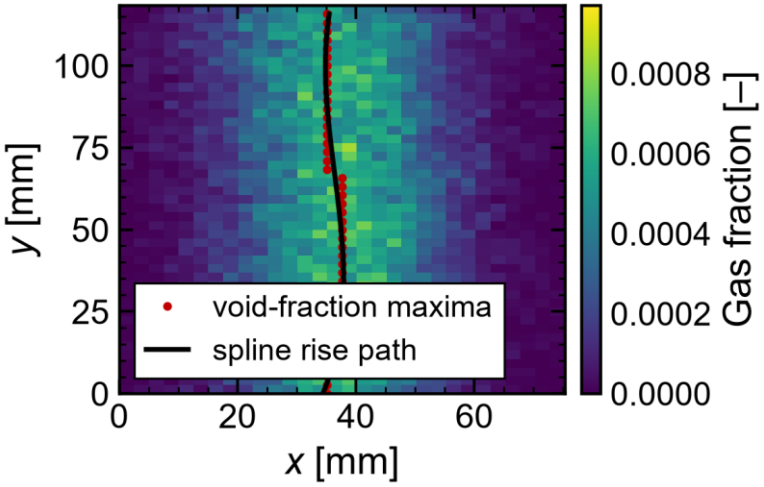
1 PSV image pairs
liquid velocity field

2 Bubble detection
ellipse axes, centroid, tilt

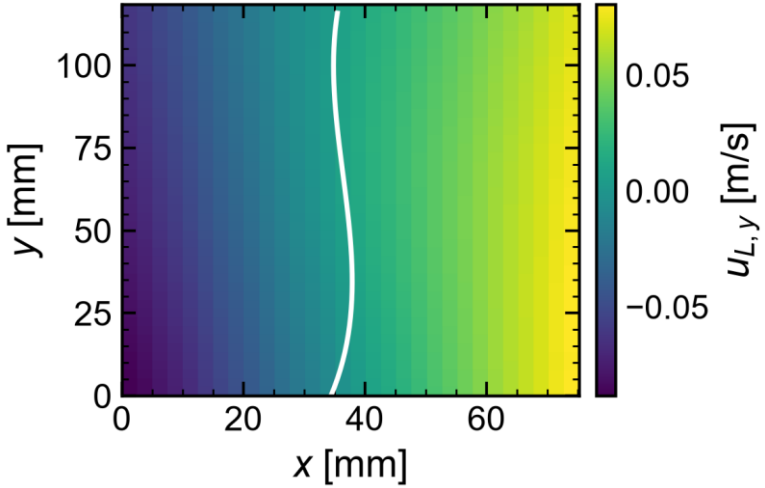
3 Tracking
pairing, velocities, IQR filter

4 Liquid field + rise path
30 × 45 grid, spline path

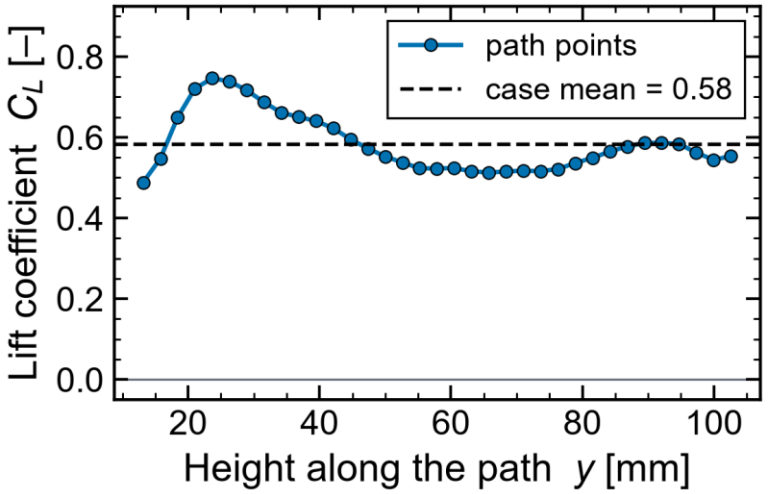
5 Force balance → C_L
35 path points per case



Mean rise path from the gas-fraction field (spline)



Time-averaged PSV liquid velocity: $u_{L,y}$ shows the linear shear



C_L along the path (35 points): the case mean is the result

Example: BMIM 1 wt %, injector inner diameter 2.8 mm, rep2. Grid 30 × 45, 25 °C properties.

Methodology: Clean-Water Reference and Groups

[1] Hessenkemper et al. 2021a
[2] Legendre & Magnaudet 1998

$$C_L = f(Sr, Re) - f(Eo_\perp)$$

$$f(Sr, Re) = \sqrt{\left(\frac{6}{\pi^2}\frac{1}{\sqrt{Re\,Sr}}\frac{2.255}{(1 + 0.2\,\varepsilon^{-2})^{3/2}}\right)^2 + \left(\frac{1}{2}\frac{Re + 16}{Re + 29}\right)^2}$$

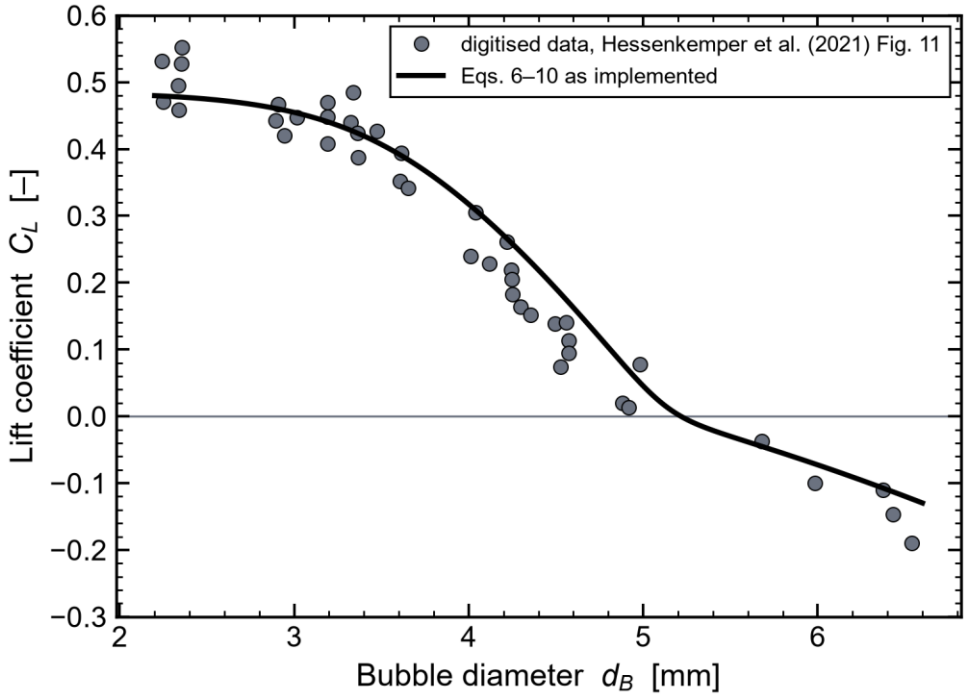
$$f(Eo_\perp) = \frac{\ln(1 + e^{-12\,G})}{12}, \qquad G = 0.11\,\frac{\ln\left(1 + e^{4(Eo_\perp - 5.6)}\right)}{4} - 0.14\,(Eo_\perp - 5.2) - 0.44$$

$$Re = \frac{\rho_L u_{slip} d_B}{\mu}, \qquad Sr = \frac{d_B \dot{\gamma}}{u_{slip}}, \qquad \varepsilon = \sqrt{Sr/Re}, \qquad Eo_\perp = \frac{\Delta\rho\, g\, {d_\perp}^2}{\sigma}$$

- Reference [1], derived in the same rig (same shear generator, PSV method, water) — no separate clean-water campaign needed
- $\Delta C_L = C_L - C_{L,Hess}$(own $Eo_\perp$, Re, Sr); $d_\perp = d_B\,E^{-1/3}$ is the major axis, E = minor/major
- f(Sr, Re) → ½ at high Re [2]; f($Eo_\perp$) produces the sign change near $Eo_\perp \approx 5.8$

Methodology: Validation and Uncertainty

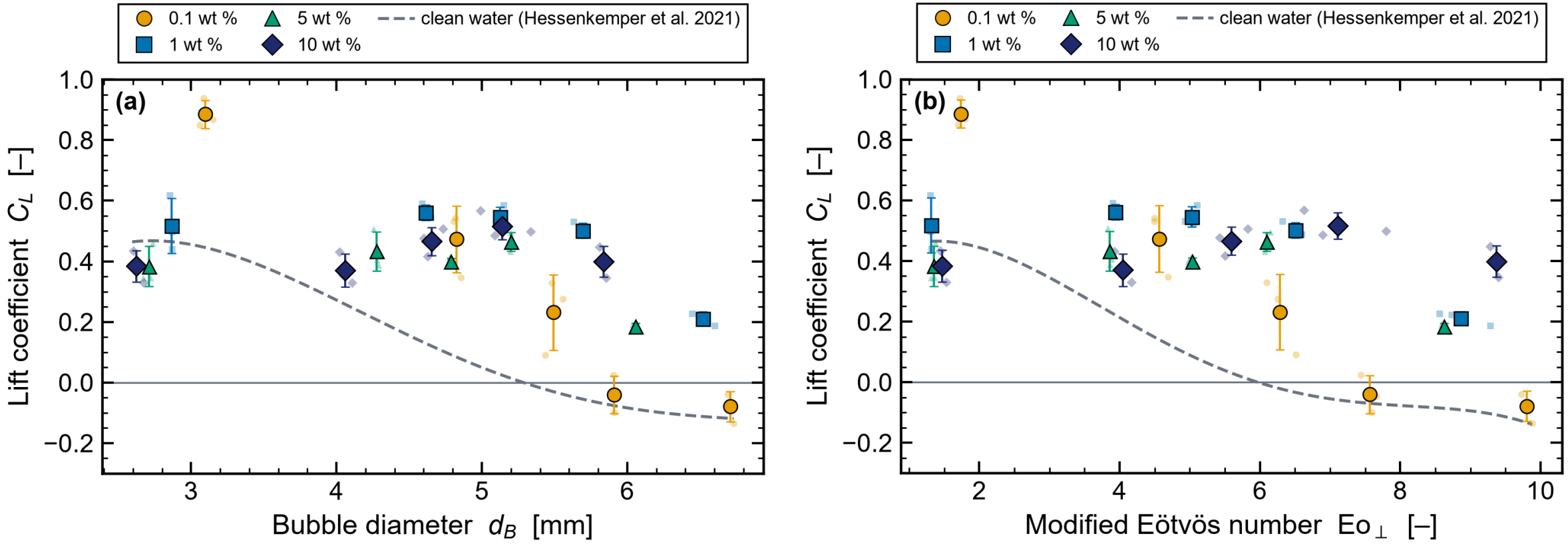
[1] Hessenkemper et al. 2021a



Digitised clean-water C_L (Fig. 11 [1]) vs Eqs. 6–10 as

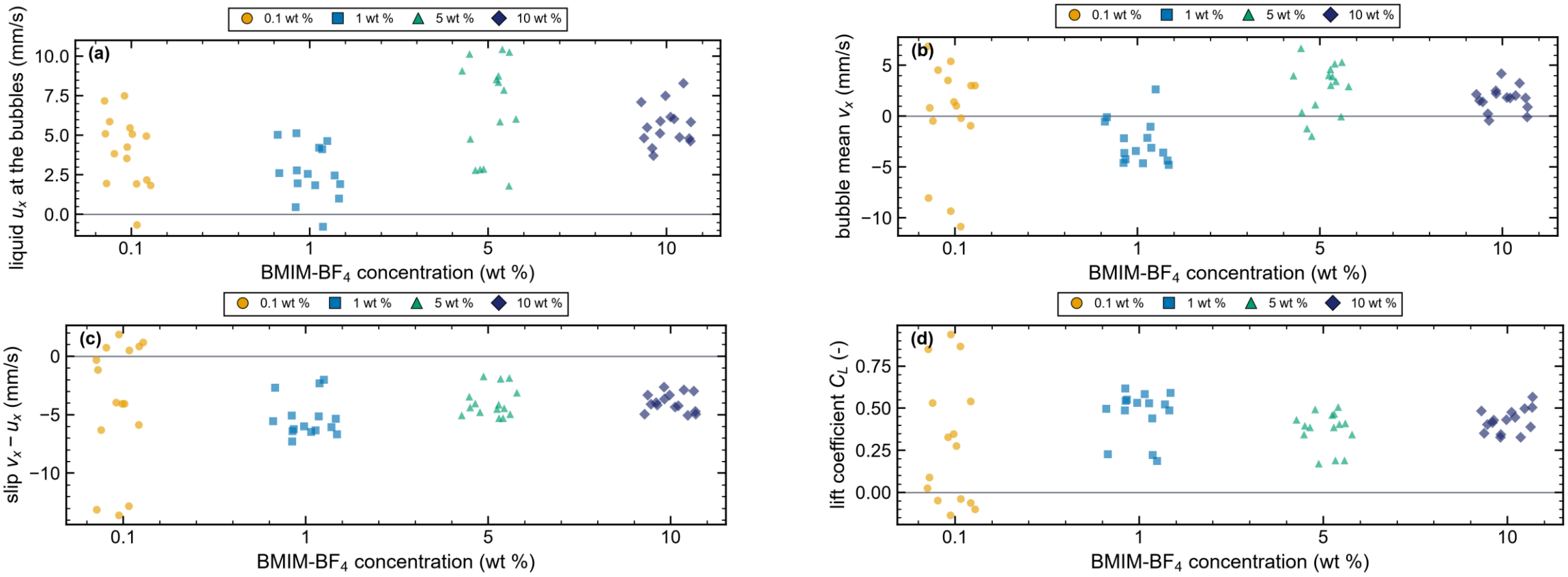
- Reproducibility, 3 repetitions: 0.047 in C_L (0.085 at 0.1 wt %)
- Grid independence: the velocity fields are averaged on a 30 × 45 cell grid; a twice finer grid (60 × 90) changes C_L by 0.013 per case (≈ 3 %)
- Largest input sensitivities: vertical bubble velocity, liquid shear / vorticity, horizontal slip bias
- Not bounded: a systematic error in the horizontal slip velocity (C_L is proportional to it: a 20 % error changes C_L by about 0.09); the assumption of a 2-D, time-averaged liquid field

Results: C_L Versus Bubble Size



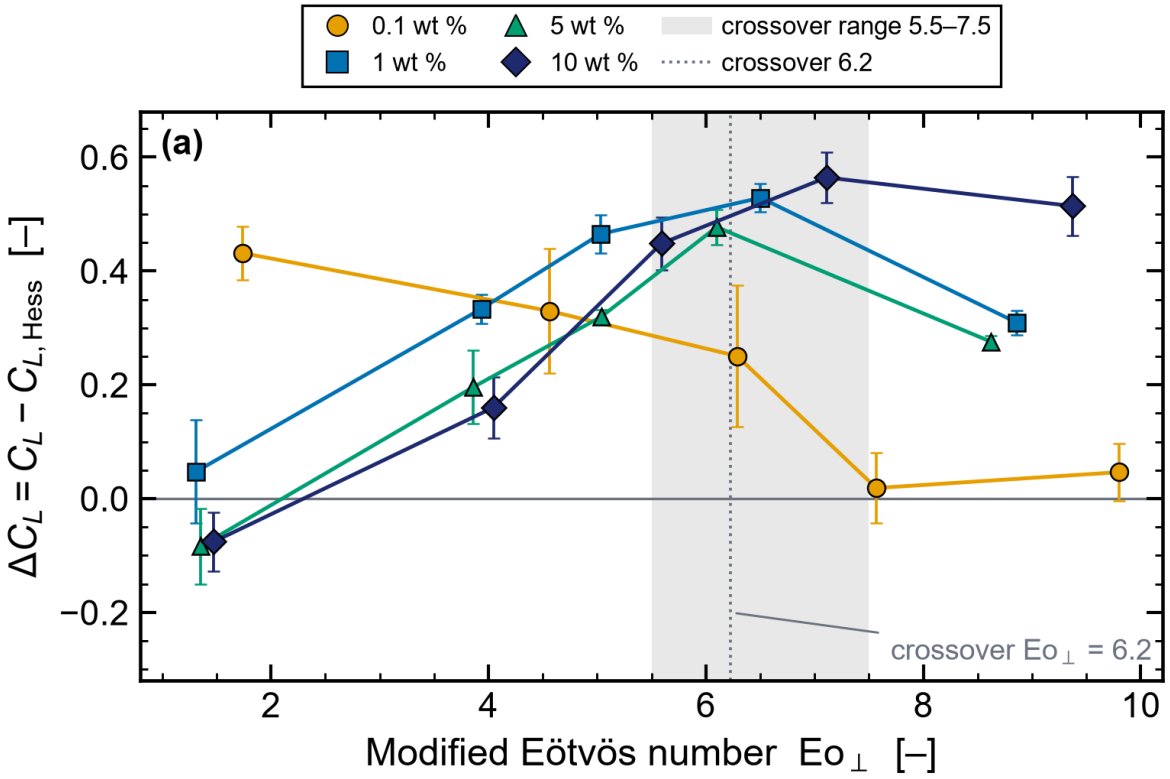
- Only 0.1 wt % crosses zero, for the two largest bubbles ($d_B \approx 5.9$ and 6.7 mm), following the clean-water reference (dashed; zero at $d_B \approx 5.2$ mm)
- 1–10 wt %: C_L stays positive (0.17–0.62) up to $Eo_\perp = 9.4$: the sign change is suppressed (the clean reference crosses zero at $Eo_\perp \approx 5.8$)
- 0.1 wt %: near-clean behaviour, reverses for the two largest bubbles ($Eo_\perp \approx 7.6$ and 9.8)

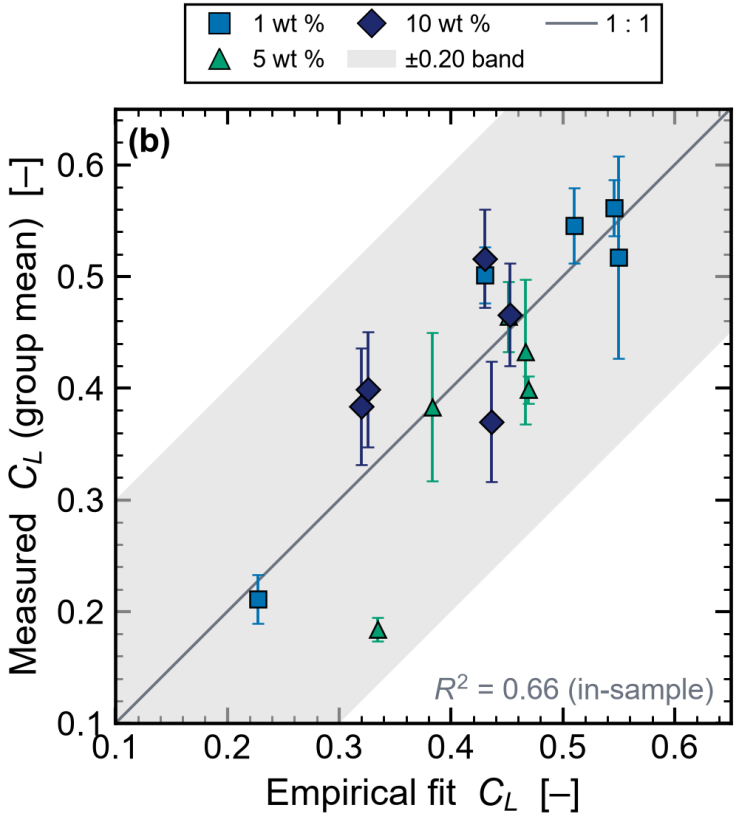
Results: Sideways Flow and Horizontal Slip



- The PSV liquid at the bubbles moves sideways at 3–7 mm/s (group means), the bubbles at −3…+3 mm/s
- The difference is the horizontal slip, about −4 to −5 mm/s at every concentration
- C_L follows the slip (r = −0.96, 60 cases): the horizontal drag term is at least 97 % of C_L
- The slip is the lateral motion the lift produces: it measures the lift, it does not explain it; the result rests on horizontal velocities (1 mm/s of slip bias = 0.09 in C_L)

Results: The Concentration Effect

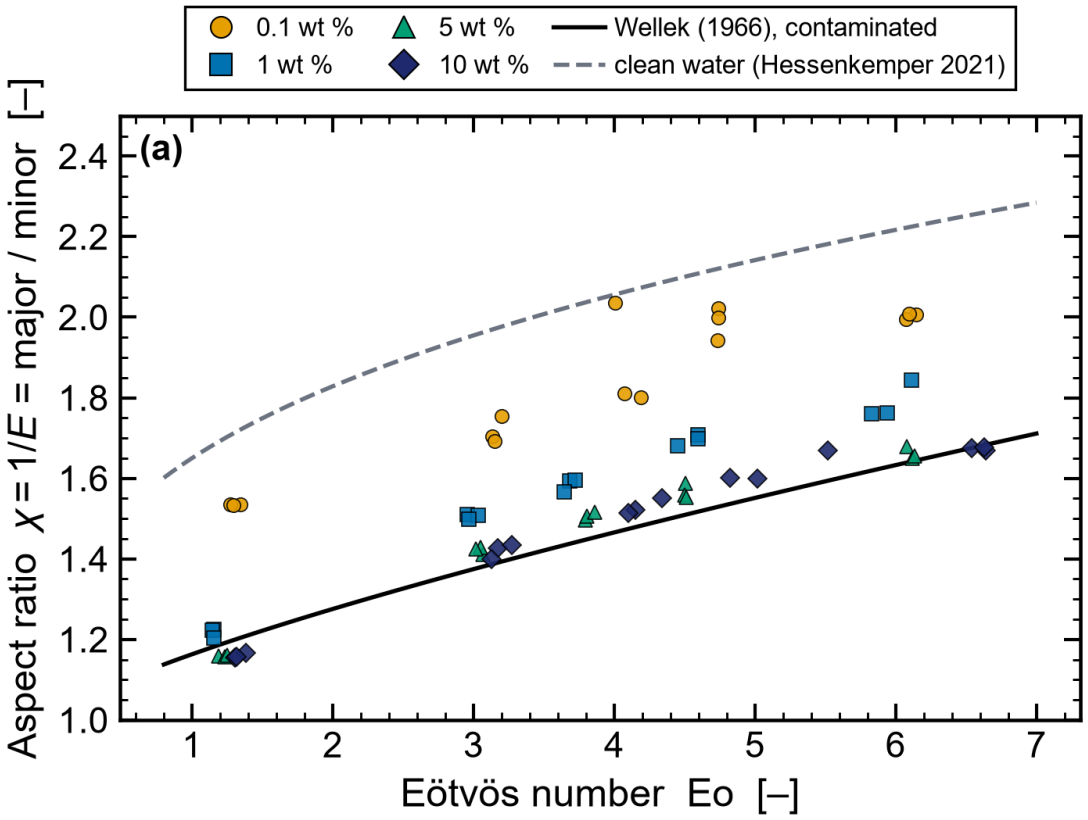


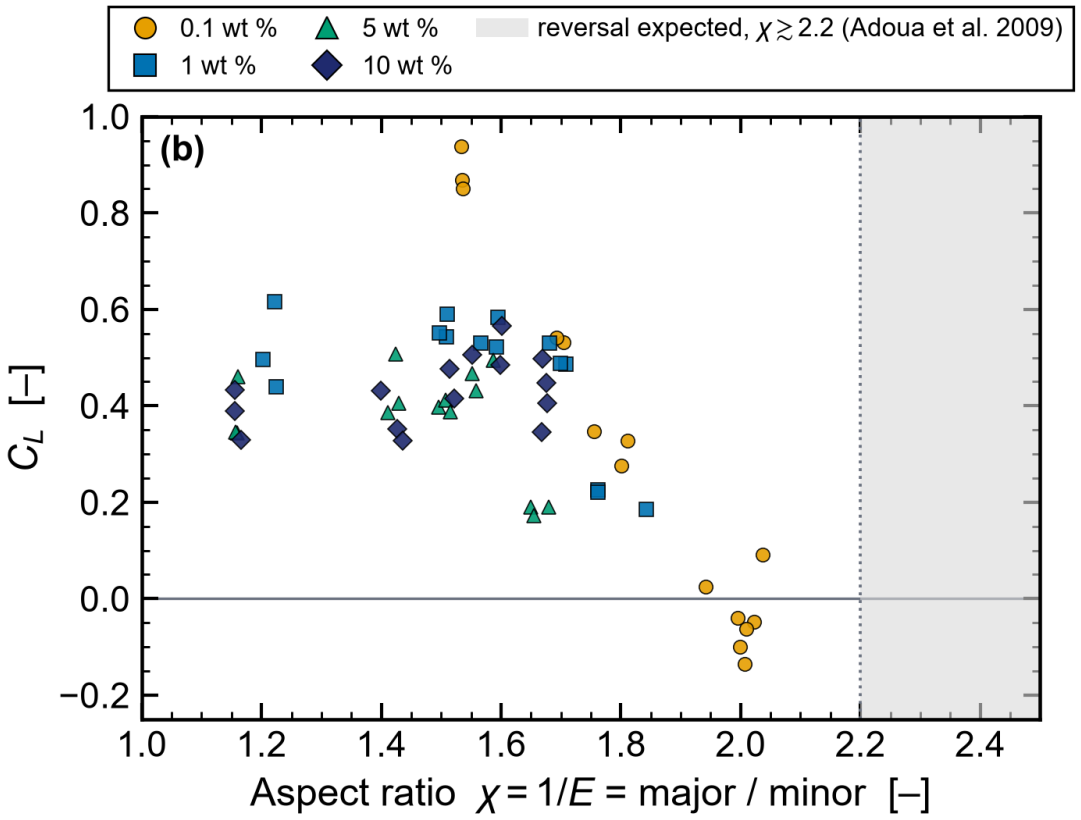


- Small bubbles: more IL lowers C_L; large bubbles: more IL raises C_L; crossover $Eo_\perp \approx 6.2$ (range 5.5–7.5)
- Empirical fit for 1–10 wt % (w = concentration in wt %): $C_L = -0.0084\,Eo_\perp^2 + 0.0422\,Eo_\perp + 0.509 + (-0.305 + 0.0491\,Eo_\perp)\log_{10} w$; R^2 = 0.66 on our own data; error for a new condition: ±0.20 in C_L

Results: Shape and the Reversal Criterion

[1] Adoua et al. 2009





- 1–10 wt %: bubbles stay less flat, near the Wellek contaminated curve; 0.1 wt %: ≈ 20 % flatter, nearer clean water
- $\chi \leq 1.85$ for 1–10 wt %, below Adoua's reversal threshold $\chi \gtrsim 2.2$ [1]; 0.1 wt % reaches $\chi = 2.0$ and reverses — but χ does not order C_L within 1–10 wt %: shape is only part of the answer

Discussion: The Critical Hatta Number

[1] Frumkin & Levich 1947; Chang & Franses 1995; Hayashi & Tomiyama 2018
[2] Scriven 1960; Lucassen-Reynders & Lucassen 1969
[3] Sadhal & Johnson 1983; Cuenot et al. 1997; Mori et al. 2024; Takagi & Matsumoto 2011

Surface stretching against adsorption: relative coverage change [1]

$$\frac{\Delta\Gamma}{\Gamma} \approx \frac{S \cdot Se}{Ha}$$

S: strain amplitude, Se = C/(C + a): surface coverage, Ha = k_{ad} C d_B / u_{slip}: adsorption rate relative to the surface flow

Marangoni stress from the coverage change [2]

$$\tau_M \sim \frac{E_G(\Delta\Gamma/\Gamma)}{d_B}$$

E_G: Gibbs elasticity from the isotherm

Viscous stress of the liquid: shear from the flow past the bubble [3]

$$\tau_{visc} \sim \frac{\mu\, u_{slip}}{d_B}$$

The surface is rigid when the Marangoni stress is at least as large as the viscous stress [3]

$$\tau_M \gtrsim \tau_{visc} \Rightarrow Ha \lesssim Ha_c = \frac{E_G\, S \cdot Se}{\mu\, u_{slip}}$$

No critical Hatta number exists in the literature: this is our order-of-magnitude scaling, without fitted parameters. It has not been validated. A possible route, yet to be checked and investigated further.

Discussion: The Limit (Sorption Kinetics)

What we know

Equilibrium: the $\sigma(C)$ isotherm gives the adsorbed amount and the Gibbs elasticity E_G

What is missing

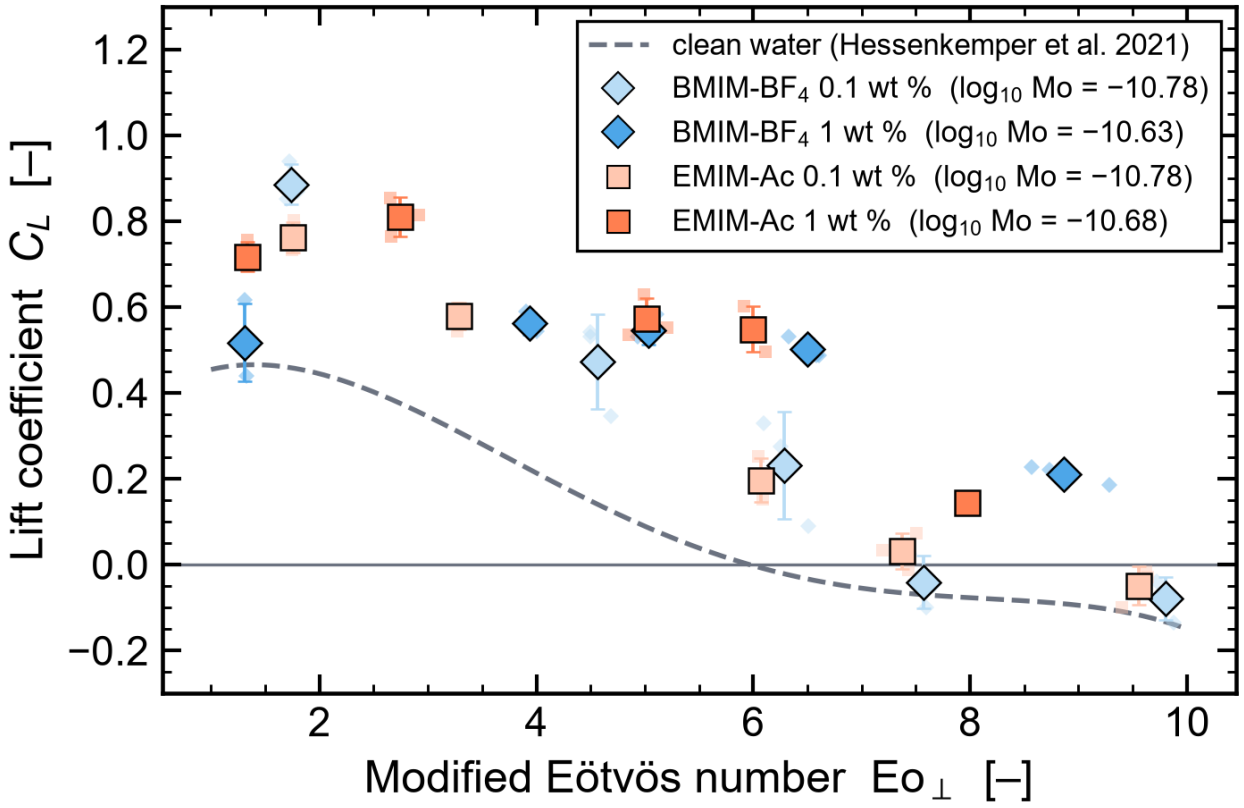
Sorption kinetics: the adsorption and desorption rate constants of BMIM-BF_4 in water are not available in the literature and were not measured here

Consequence

Without them the Hatta number cannot be evaluated: whether the interface is immobilised cannot be decided in this study

Open: is the change of C_L an interface or a bulk-property effect?

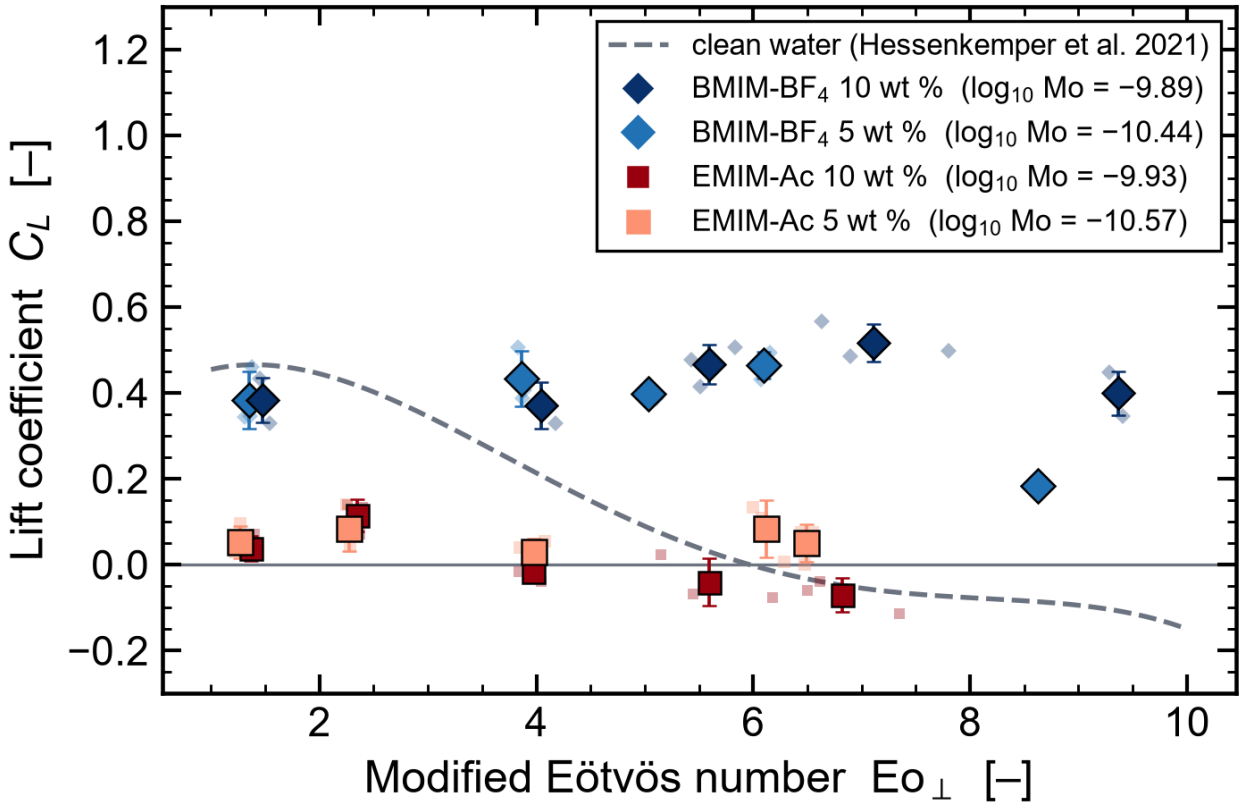
Discussion: Bulk or Interface? EMIM-Ac at 0.1 and 1 wt %



- Low concentrations: EMIM-Ac and BMIM-BF_4 have almost the same Morton number, and the surface tension of both is close to water
- EMIM-Ac, 30 cases (0.1 and 1 wt %): it reproduces BMIM-BF_4. At 0.1 wt % both reach $C_L \approx 0$ near $Eo_\perp \approx 7.5$
- At 1 wt % both stay positive (EMIM 0.14–0.85, BMIM 0.19–0.62) and fall for the largest bubbles; EMIM-Ac is 0.2–0.25 higher for the small bubbles
- **Similar properties, similar behaviour**

EMIM-Ac: 0.1 wt %, 15 cases (water properties, approximation); 1 wt %, 15 cases. Three repetitions at each of the five sizes; group means ± SD.

Discussion: Bulk or Interface? The EMIM-Ac Comparison

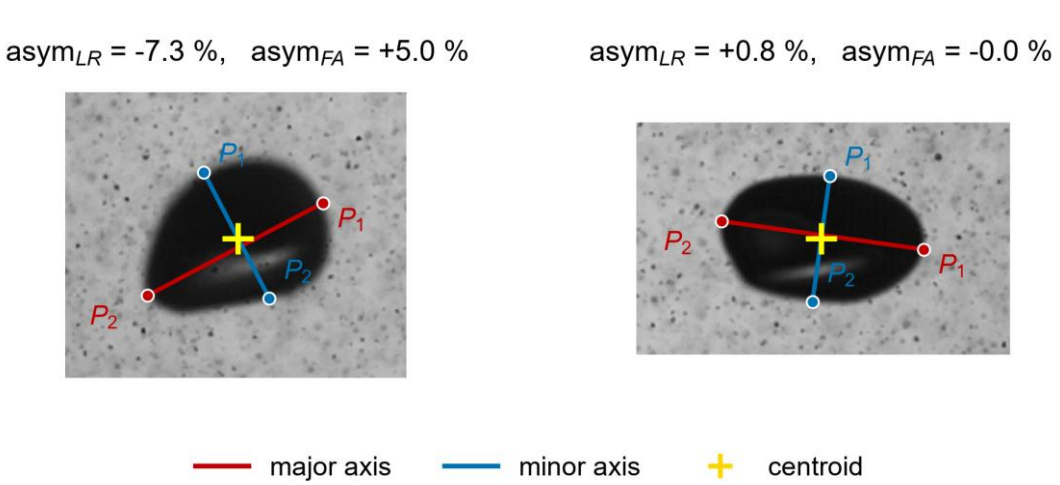


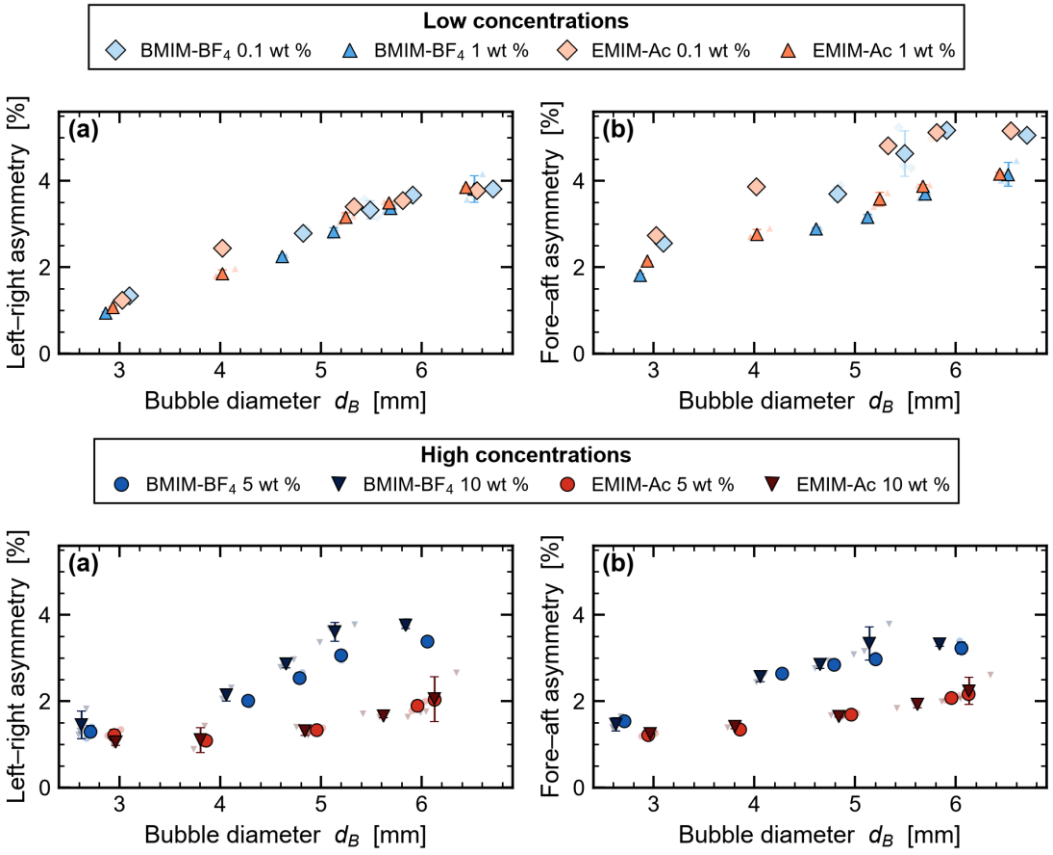
- Second ionic liquid EMIM-Ac: same Morton number as BMIM at the same concentration, almost no surface activity
- EMIM-Ac, 30 cases (10 and 5 wt %): C_L = −0.12…+0.14 vs 0.17–0.57 for BMIM 5–10 wt %: matched Mo does not reproduce BMIM
- EMIM reverses at $\chi \approx 1.4$ — the aspect-ratio argument does not carry over
- **Open: separate surface activity from bulk properties (EMIM-Ac differs in both)**

EMIM-Ac: 10 and 5 wt %, 15 cases each (three repetitions at each of the five sizes).

Discussion: Other Candidate Mechanisms

[1] Hidman et al. 2022; Adoua et al. 2009



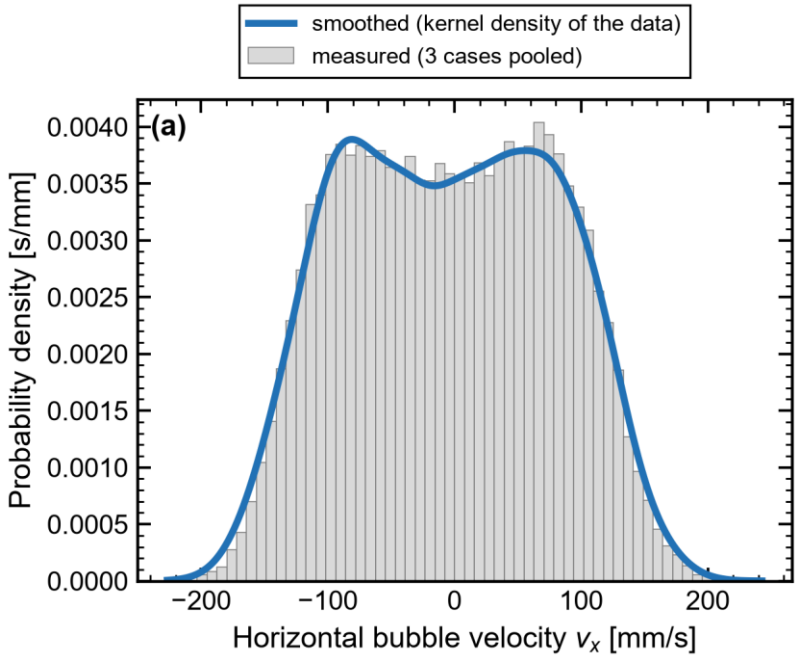


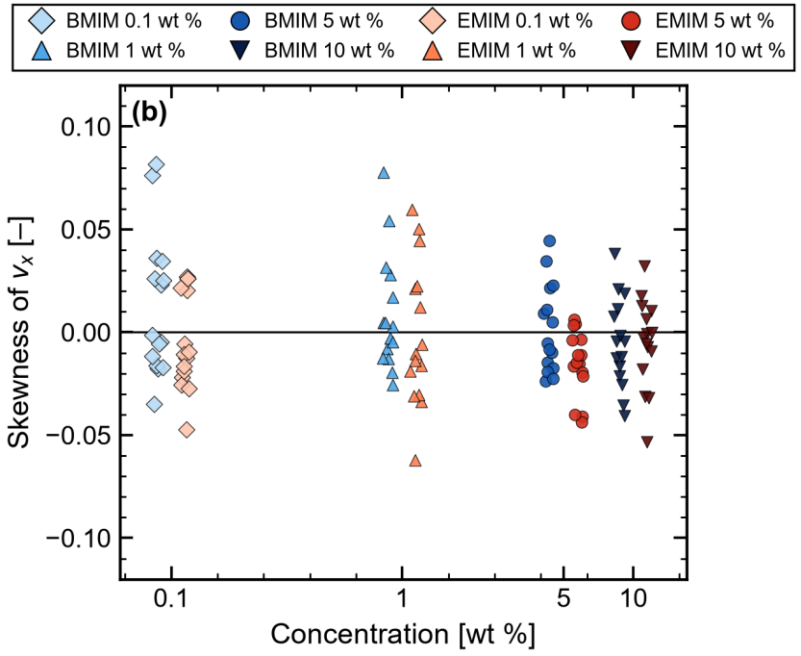
- Asymmetry = how far the centroid lies from the middle of each fitted axis: $(d_1 - d_2)/(d_1 + d_2)$
- Literature [1]: asymmetric deformation gives negative lift at low-to-moderate Galilei number, $Ga = \rho_L\sqrt{(g\, d_B^3)}/\mu_L$ (buoyancy to viscous forces); ours is Ga ≈ 360–1900 (surface-vorticity and wake mechanisms)

- Asymmetry grows with bubble size in both liquids; at the same size EMIM-Ac bubbles are 35–45 % less asymmetric at 5 and 10 wt %, and as asymmetric as BMIM-BF$_4$ at 0.1 and 1 wt %
- In BMIM-BF$_4$ it is mainly a size variable: adding it improves the fit of the group means, not the prediction for an unseen injector size

Discussion: Symmetric Two-Peak Path Motion

[1] Hessenkemper et al. 2021b





- Measured: two peaks, symmetric about the mean (BMIM-BF4 at 1 percent with the 4 mm bubble)

- Skewness = how one-sided the distribution is (0 = symmetric)
- All 120 cases are within ±0.08

Wake: Hessenkemper et al. [1] observed a one-sided two-peak distribution for partly contaminated bubbles and suggested an asymmetric wake as a possible explanation (the wake was not measured). We see no one-sided distortion. This is a sign of a symmetric wake, not a proof: the near wake and the 3-D path were not studied (they need a second view plane, finer PSV near the bubble, or DNS).

Conclusions and Outlook

Conclusions

- In BMIM-BF_4 at 1–10 wt % the lift sign change is suppressed: C_L stays positive (0.17–0.62) up to $Eo_\perp = 9.4$
- Between the concentrations: for small bubbles more ionic liquid lowers C_L, for large bubbles it raises C_L; the two effects cross at $Eo\perp \approx 6.2$; an empirical fit describes the data (±0.20 for new conditions)
- Shape is only part of the answer; the role of the interface cannot be decided without the sorption kinetics (not available)
- Asymmetric deformation is mainly a size effect; the near-bubble wake was not studied (needs 3-D or DNS)

Outlook

- Interpret the Morton-matched EMIM-Ac comparison (10 and 5 wt %): bulk vs interfacial effects
- Determine the sorption kinetics (molecular dynamics) to evaluate the critical Hatta number
- More sizes per concentration, and literature C_L data, to turn the fit into a predictive closure
- Second view plane and finer PSV near the bubble: near wake and 3-D path (not resolved here)

References

Motivation: bubble columns, regimes, closures

Besagni, G., Inzoli, F., De Guido, G., Pellegrini, L.A. (2017) Chem. Eng. Sci. 158, 509–538.

Lucas, D., Prasser, H.M., Manera, A. (2005) Chem. Eng. Sci. 60(13), 3609–3619.

Lucas, D., Ziegenhein, T. (2019) Int. J. Multiph. Flow 120, 103092.

Shah, Y.T., Kelkar, S.P., Godbole, S.P., Deckwer, W.D. (1982) AIChE J. 28(3), 353–379.

Tomiyama, A., Tamai, H., Zun, I., Hosokawa, S. (2002) Chem. Eng. Sci. 57, 1849–1858.

Concepts and physics of lift

Auton, T.R. (1987) J. Fluid Mech. 183, 199–218.

Legendre, D., Magnaudet, J. (1998) J. Fluid Mech. 368, 81–126.

Magnaudet, J., Eames, I. (2000) Annu. Rev. Fluid Mech. 32, 659–708.

Mori, T., Igarashi, R., Hayashi, K., Kurimoto, R., Tomiyama, A. (2024) Chem. Eng. Res. Des. 204, 343–353.

Adoua, R., Legendre, D., Magnaudet, J. (2009) J. Fluid Mech. 628, 23–41.

Hidman, N., Ström, H., Sasic, S., Sardina, G. (2022) J. Fluid Mech. 952, A34.

Tagawa, Y., Takagi, S., Matsumoto, Y. (2014) J. Fluid Mech. 738, 124–142.

Contamination, interface and properties

Cuenot, B., Magnaudet, J., Spennato, B. (1997) J. Fluid Mech. 339, 25–53.

Takagi, S., Matsumoto, Y. (2011) Annu. Rev. Fluid Mech. 43, 615–636.

Hayashi, K., Legendre, D., Tomiyama, A. (2020) Int. J. Multiph. Flow 129, 103350.

Hessenkemper, H., Ziegenhein, T., Lucas, D., Tomiyama, A. (2021b) Int. J. Multiph. Flow 145, 103833.

Lewandowski, B., Fertig, M., Ulbricht, M., Krekel, G. (2019) Chem. Eng. Sci. 199, 179–198.

Lucassen-Reynders, E.H., Lucassen, J. (1969) Adv. Colloid Interface Sci. 2, 347–395.

Szyszkowski, B. von (1908) Z. Phys. Chem. 64, 385–414.

Sarraute, S., Costa Gomes, M.F., Pádua, A.A.H. (2009) J. Chem. Eng. Data 54, 2389–2394.

Methods and reference correlations

Ziegenhein, T., Tomiyama, A., Lucas, D. (2018) Int. J. Multiph. Flow 108, 11–24.

Hessenkemper, H., Ziegenhein, T., Lucas, D. (2020) Chem. Eng. J. 386, 121589.

Hessenkemper, H., Ziegenhein, T., Rzehak, R., Lucas, D., Tomiyama, A. (2021a) Int. J. Multiph. Flow 138, 103587.

Wellek, R.M., Agrawal, A.K., Skelland, A.H.P. (1966) AIChE J. 12, 854–862.

Thank you for your time and your attention.

Acknowledgment

This work has been financed by the Italian Ministry of University and Research (Ministero dell'Università e della Ricerca) within the FIS2 call. In particular, this work has been conducted within the AURIGA ("Unveiling the Riddles of Gas liquid fluid dynamics: towards novel carbon dioxide absorption systems") project. Project number FIS-2023-00204, CUP D53C25000730001, funded within the FIS2 call (Decreto Direttoriale n. 1236 del 1-08-2023).

djameleddine.aissaoui@polimi.it

Department of Energy, Politecnico di Milano
AURIGA project – FIS-2023-00204
www.polimi.it

CHECK OUR WEBSITE